Electronic Supplementary Material (ESI)

Quercetin dual interaction at the membrane level

António de Granada-Flor [a †], Carla Sousa [a †], Hugo A. L. Filipe [b, c], M. Soledade C. S. Santos [a], Rodrigo F. M. de Almeida[a]*

[a.] Centro de Química e Bioquímica, Centro de Química Estrutural, Departamento de Química e Bioquímica, Faculdade de Ciências, Universidade de Lisboa, Ed. C8, Campo Grande, 1749-016 Lisboa, Portugal.
[b.] Coimbra Chemistry Center, University of Coimbra, P-3004-535 Coimbra, Portugal
[c.] CNC – Center for Neuroscience and Cell Biology, University of Coimbra, P-3004-517 Coimbra, Portugal

† These authors contributed equally.

Materials and Methods

Materials. 1-palmitoyl-2-oleoyl-*sn*-glycero-3-phosphocholine (POPC), *N*-palmitoyl-sphingomyelin (PSM) and 1,2-dioleoyl-*sn*-glycero-3-phosphoethanolamine-*N*-(7-nitrobenz-2-oxa-1,3-diazol-4-yl) (NBD-DOPE) were obtained from Avanti Polar Lipids. 1-[4(trimethylammonio)phenyl]–6-phenylhexa-1,3,5-(all-*trans*)-triene (TMA-DPH) *p*-toluenesulfonate was from Invitrogen. Quercetin (96%), Cholesterol (Chol) and all other reagents, analytical or spectroscopic grade (solvents) were obtained from Sigma-Aldrich.

Large unilamellar vesicles (LUV) preparation. LUV were prepared following a previously described procedure.[1] In brief, the required volume of a lipid stock solution was added to a vial in order to obtain the desired final lipid concentration. The solvent was evaporated with a mild, continuous flow of nitrogen, followed by overnight vacuum. Whenever required, two identical lipid mixtures were prepared, one without probe (blank), and one with the adequate volume of fluorescent probe in organic solvent (methanol), added to the lipid mixture at 1:500 probe: lipid molar ratio, before the solvent evaporation step. After hydration with buffer (10 mM HEPES (4-(2-hydroxyethyl)-1-piperazineethanesulfonic acid); pH 7.4; 150 mM NaCl) pre-warmed at 60 °C, samples were submitted to vortex stirring and freeze thaw cycles. LUV suspensions were formed by extrusion (Avanti Mini-extruder) at 60 °C, by forcing the multilamellar vesicle suspension 21 times through polycarbonate filters with 100 nm diameter pores (Nuclepore, Whatman) and left to equilibrate overnight.

The interaction of quercetin (QCT) with lipid bilayers was studied in LUV suspensions using three different lipid systems at 23 °C: POPC (single l_d phase), POPC/Chol 1:1 (single l_o phase), and POPC/PSM/Chol with several molar ratios spanning the tie-line containing the equimolar proportion of the lipids.[2]

Steady-State and time resolved fluorescence. QCT partition to POPC, POPC/Chol and POPC/PSM/Chol was determined using QCT intrinsic fluorescence, maintaining flavonoid concentration constant (at 8 µM or 20 µM) (1.6% DMSO, v/v), while increasing lipid concentration. Steady state anisotropy is given by:[3]

$$<r> = \frac{I_{VV} - GI_{VH}}{I_{VV} + 2GI_{VH}} \quad (1)$$

where G is a correction factor obtained from I_{HV}/I_{HH}. I_{ij} is the measured fluorescence intensity and subscripts V and H represent the vertical and horizontal orientations of the polarizers (i. excitation, j. emission).

QCT was incubated with lipid systems at 23 °C for at least 2 hours. The use of fluorescence anisotropy to determine partition coefficients presents several advantages, namely: it is largely insensitive to inner filter effects, and since it is a parameter intrinsically corrected for total fluorescence intensity (eq 1), it does not depend on the exact QCT concentration.[4] For the calculation of K_p, I_w and I_L were estimated from the total emission intensity at the magic angle (given by $I_{VV} + 2GI_{VH}$) in water (buffer) and in lipid (for the highest lipid concentration used), respectively. The average lipid molar volume was taken as 0.795 dm³/mol for POPC[1], 0.558 dm³/mol for POPC/Chol (1:1) (obtained considering an average area per lipid and a bilayer thickness of 41.8 Å² and of 2.2 nm, respectively), 0.715 dm³/mol for POPC/PSM/Chol 72:23:5 (obtained considering an average area per lipid of 55.7 Å² and a bilayer thickness of 2.1 nm) and 0.558 dm³/mol for POPC/PSM/Chol 25:35:40 (obtained considering an average area per lipid of 37.0 Å² and a bilayer thickness of 2.5 nm)[5, 6]. QCT

partition between l_d and l_o phases was inspected using LUV of POPC/PSM/Chol, varying the mole fraction of l_o phase between 0 and 1. The total lipid concentration was 1 mM guaranteeing that most QCT was incorporated in the lipid bilayer in the l_d phase. QCT concentration was 20 µM, to minimize signal interferences without altering membrane biophysical properties.

To obtain the quantitative value of the mole fraction $K_p^{ld/lo}$, the membrane/water partition coefficients in the ternary system for the two extremes of the tie-line, 100% l_d and 100% l_o, were obtained as described for POPC and POPC/Chol. Then, these values were converted to mole fraction partition coefficients, through the expression

$$K_{px} = K_p \frac{V_L}{V_W} \qquad (2)$$

In this situation, the following relationship holds (when interfacial effects are negligible):

$$K_{px}^{ld/lo} = K_{px}^{ld/water} / K_{px}^{lo/water} \qquad (3)$$

where $K_{px}^{ld/lo}$ is the mole-fraction partition coefficient between ordered and disordered phases.

A Horiba Jobin Yvon Spex Fluorolog 3-22 spectrofluorimeter was used, and the experiments were conducted under controlled temperature at 23 ± 1 °C with quartz cuvettes using a 0.4 x 1.0 cm (or, when required, 0.2 x 1.0 cm) excitation-emission pathway in order to minimize polyphenol absorption and vesicles light scattering, ensuring that fluorescence intensity is proportional to absorption and that there are no inner filter effects. All intensity readings were blank corrected. QCT emission spectra were measured with excitation wavelength (λ_{ex}) at 367 nm.

Quenching experiments of QCT fluorescence were performed with 20 µM QCT and increasing concentrations of acrylamide or KI, using 11 nm slits. Whenever required, the KI solution contained sodium dithionite at 1 mM.

The effects of 80 µM QCT on membrane biophysical properties were assessed in three lipid systems with 2 fluorescent membrane probes (TMA-DPH and NBD-DOPE) in similar conditions as for K_p determination. TMA-DPH fluorescence lifetime is very sensitive to changes in membrane hydration, reporting an increased water penetration through a drastic reduction in its fluorescence lifetime (due to the appearance of a short lifetime component). NBD-DOPE has a more superficial location than TMA-DPH and can be used to probe changes in membrane surface fluidity in a straightforward manner through its steady-state fluorescence anisotropy. NBD-DOPE steady state fluorescence anisotropy was measured with λ_{ex} at 468 nm and λ_{em} at 536 nm, using 4 nm and 10 nm slits in the excitation and emission paths, respectively.

For time-resolved measurements by the single photon counting technique, λ_{ex} at 460 nm (using a nanoLED source model N-460; Horiba Jobin-Yvon) and λ_{em} at 536 nm (14.7 nm slits) were used for NBD-DOPE. TMA-DPH measurements were performed with λ_{ex} at 370 nm (using a nanoLED source model N-370 plus a UGI-370 band pass filter; Horiba Jobin-Yvon) and λ_{em} at 450 nm with 2.5 nm slits. The same nanoLED was used for QCT decay measurements, but with a 548 nm λ_{em}. QCT does not interfere with TMA-DPH fluorescence as previously reported by Margina and collaborators.[7]

Ludox (colloidal silica diluted to 50% v/v in water) was used as the scatterer to obtain the instrument response function. The analysis of the experimental fluorescence decays was carried out with the program TRFA data processor version 1.4 (Minsk, Belarus) with a non-linear least squares fitting method, based on Marquardt's algorithm, and the fit quality judged in compliance with reduced χ^2, visual inspection of weighted residuals and auto correlation distribution. Fluorescence intensity decays were described by a sum of exponentials of the type:[3]

$$I(t) = \sum_{i=1}^{n} \alpha_i \, exp(-t/\tau_i) \quad (4)$$

Where α_i is the normalized amplitude and τ_i is the corresponding lifetime of component i. For such decay law, the intensity-weighted mean fluorescence lifetime is given by:[3]

$$<\tau> = \sum \alpha_i \tau_i^2 / \sum \alpha_i \tau_i \qquad (5)$$

The denominator in the previous expression is the amplitude-weighted mean fluorescence lifetime, $\bar{\tau}$.

Molecular Dynamics (MD) simulations. MD simulations and analysis of trajectories was carried out using the GROMACS 5.1.4 package.[68] The GROMOS 54A7 force field [9-11] was used together with the SPC water model.[12] An initial topology for QCT was obtained with the Automated Topology Builder (ATB) and Repository [13, 14] and manually curated. MD simulations were performed only with neutral QCT species, i.e., the fully protonated form at the top left of Fig. S1. The charge set for the molecule was derived from ab initio quantum mechanical calculations.[15] The needed electrostatic potential was calculated in structures optimized using Gamess-US [16, 17] using the B3LYP functional [18-20] and 6-31G* [21] basis set. The final topology of QCT is available below. Figure S1 shows structures and numbering of relevant atoms of POPC and QCT molecules.

Bilayers containing 4 QCT molecules were obtained by randomly inserting the molecules inside equilibrated lipid bilayers[22] without replacement of lipids. The pure POPC bilayer is composed by 128 lipids hydrated by 5143 water molecules, while that of POPC/Chol 1:1 is composed by 144 lipids hydrated by 5824 water molecules. For each lipid composition, POPC and POPC/Chol, three different simulations were performed, two with molecules starting at different positions at the lipid/water interface (2 molecules in each leaflet) and the other with the four QCT molecules in the centre of the bilayer. In all systems, unfavourable atomic contacts were removed by steepest descent energy minimization. For each system, a short (100 ps) MD run was then carried out using a 1 fs integration step, followed by a 400 ns run using a 2 fs integration step. Bond lengths were constrained to their equilibrium values, using the SETTLE algorithm [23] for water and the LINCS algorithm [24] for all other bonds. All simulations were carried out under constant number of particles, pressure (1 bar) and temperature (298.15 K), and with periodic boundary conditions. Pressure and temperature control were carried out using the weak-coupling Berendsen scheme,[25] and V-rescale [26] thermostat with coupling times of 1.0 ps and 0.1 ps, respectively. Semiisotropic pressure coupling was used. Van der Waals interactions were cut off at 1.0 nm. Coulomb interactions were calculated using the Particle Mesh Ewald method,[27] with a cut-off of 1.0 nm for the real space component. For visualization of structures and trajectories, Visual Molecular Dynamics software (University of Illinois) was used.[28] For each lipid composition, POPC or POPC:Chol, the first 150 ns (170 ns) of each simulation were used for equilibration, and the remaining 250 ns (230 ns) were used for analysis.

Other procedures. Phospholipid concentration (POPC; PSM) was determined by inorganic phosphate quantification[29] and Chol quantification was made by gravimetry (Mettler Toledo, XS 205 dual range balance; d=0.01 mg). Probe concentrations in stock solutions (spectroscopic grade solvents) were determined spectrophotometrically using $\varepsilon = 21 \times 10^3$ M^{-1}cm^{-1} (NBD-DOPE, λ_{max}=458 nm, chloroform stock solutions)[30] and $\varepsilon = 80 \times 10^3$ M^{-1}cm^{-1} (TMA-DPH, λ_{max}=350 nm, methanol).[31]

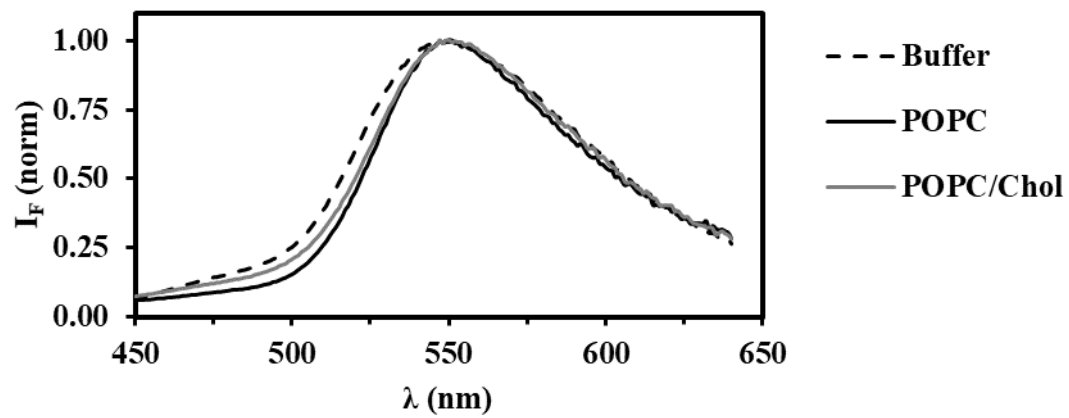**Note 1. Emission spectra of quercetin in aqueous and lipid environments**

Since QCT has several (5) ionizable hydroxyl groups[32-34] (Figure S1) it is important to consider its ionization state, so as to properly understand to which QCT form the K_p values retrieved correspond. According to literature, QCT has a pK_{a1} of 7.1 at 50 mM ionic strength, essentially assigned to the ionization of the A ring OH group in position 7 (Figure S1).[33] As a result, near physiological ionic strength (150 mM), the calculated thermodynamic pK_{a1} is 7.06. In these conditions 67% of QCT is ionized at pH 7.4. A study of QCT ionization dependency on pH and the corresponding excitation/emission fluorescence spectra shows that for pH 7.0 or higher, QCT emission has a major peak at ~535 nm, assigned to its ionized form.[35]

Figure S2 shows the QCT fluorescence emission spectra (pH 7.4), as it partitions to POPC and POPC/Chol LUV, where it is clear that only one major peak at ca. 550 nm is detectable. Moreover, the use of a more polar co-solvent in this work (1.6% DMSO) justifies the red-shift relative to the spectra reported by Mezzetti and co-workers[35] (10% methanol), indicating that at this wavelength only the distribution of monoionized QCT is being monitored.

The absence of any noticeable changes on the emission and the excitation/absorption spectra envelope denotes that the interaction with the membrane is essentially not shifting the ionization equilibrium of the molecule, and therefore it is reasonable to assume an analogous distribution of the ionized and neutral forms, justifying the simple partition model for K_p calculation. QCT has an extensive double-bond conjugation system (Figure S1), and although an increase in QCT pK_a upon membrane interaction cannot be completely ruled-out,[36] charge delocalization softens the ionization state effects associated with QCT insertion into the lipid bilayer. A careful inspection of the spectra shows that the main band, corresponding to the ionized form, is maintained (POPC/Cholesterol) or even intensified (POPC) upon QCT insertion into the membrane while the band below 500 nm, corresponding to the neutral form, is less intense than in buffer.
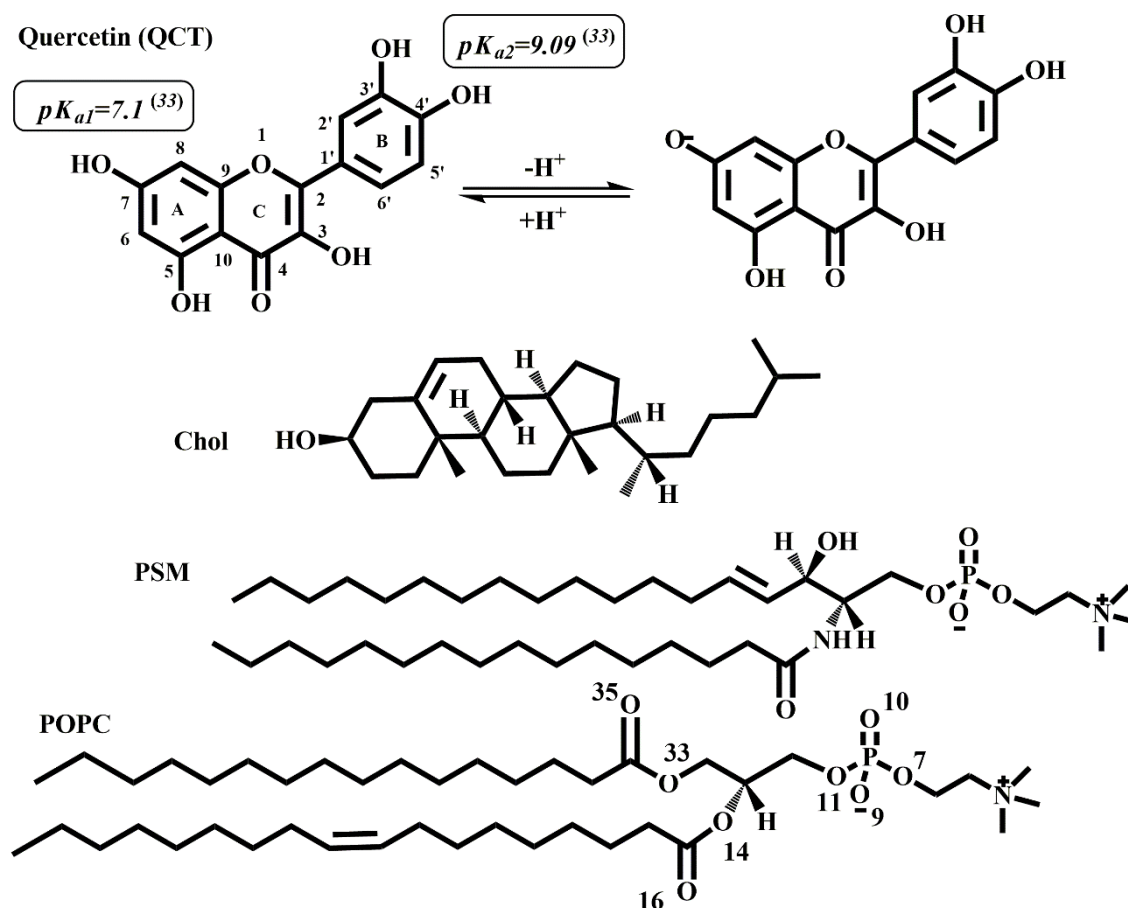
Figure S1. Chemical structures of lipids and quercetin. pK_{a1} and pK_{a2} of the main functional groups that can ionize at physiological pH according to Herrero-Martínez et al., 2005.[33] The numbering of the oxygen atoms in POPC is the one used for the presentation of MD simulations results.

Figure S2. Normalized emission spectra of quercetin in buffer and upon partitioning to LUV (1 mM total lipid) of POPC and POPC/Chol 1:1 mol/mol.
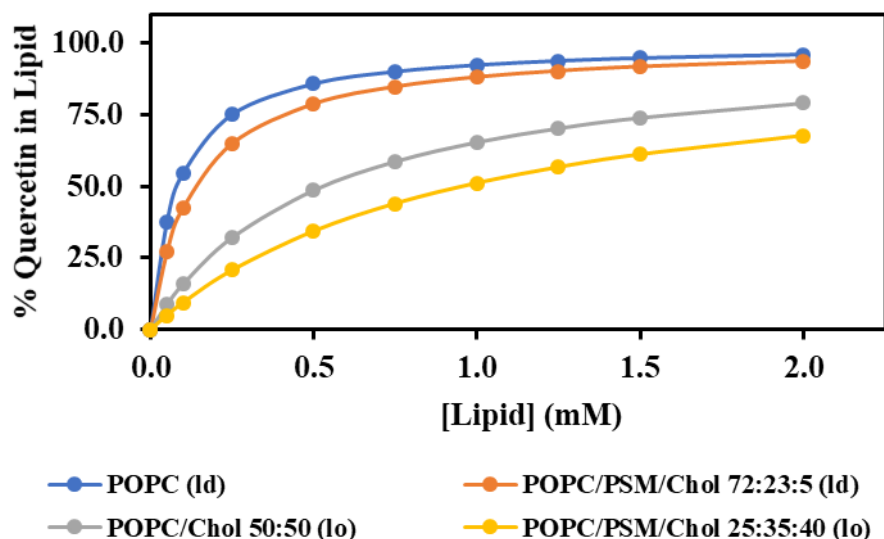
Note 2. Quercetin partition to lipid bilayers

Figure S3. Quercetin mole% in each lipid system upon membrane partition.

Table S1. Mole fraction partition coefficients in the different lipid systems for polyphenols and a membrane probe. The fluorescence intensity ratio between lipid and water of quercetin needed for K_p calculations is also provided.

Phase (i)	I(i)/Iw	K_{px}		
	Quercetin	Quercetin	*Rosmarinic acid*[1]	**di-4-ANEPPS**[37, *a*]
l_d (POPC)	1.21 ± 0.21	$(6.69 \pm 0.79) \times 10^5$	$(2.25 \pm 0.61) \times 10^4$	6.6×10^5
l_o (POPC/Chol 1:1)	1.09 ± 0.07	$(1.12 \pm 0.37) \times 10^5$	4.2×10^3	1.1×10^6
l_d (POPC/PSM/Chol, 72:23:5)	1.33 ± 0.05	$(4.11 \pm 0.64) \times 10^5$	-	
l_o (POPC/PSM/Chol, 25:35:40)	1.03 ± 0.09	$(5.81 \pm 0.54) \times 10^4$	-	

aThe sterol used to form the lo phase was ergosterol.

The mole-fraction partition coefficients of QCT between pure l_d or l_o phases and water is presented in Table S1. These values are higher than those recently reported for the more hydrophilic rosmarinic acid, a polyphenol of the hydroxycinnamic acid family[1]. QCT K_p in the l_d (POPC) phase is also similar to that reported for a fluorescent membrane probe di-4-ANEPPS[37] and lies between the values obtained for substituted lipid chain NBD probes which have l_d /water partition coefficients between 1×10^3 and 1×10^5, depending on carbon chain length.[38]

The experimental values of anisotropy along the l_d / l_o tie-line in Fig. 1B (main text) can be accurately reproduced with a calculation using: $<r_{lo}>$ and $<r_{ld}>$, i.e., the steady-state fluorescence anisotropy values of QCT in each lipid phase (in the extremes of the tie-line), membrane/water K_{px}, the mole-fraction partition coefficient between ordered and disordered phases, I_{lo}/I_{ld}, the ratio of fluorescence intensity of QCT in each lipid phase and the fraction of QCT in water and $<r_w>$, as function of X_{lo}, the liquid ordered mole-fraction. This indicates that l_d / l_o domain interfaces are not preferentially occupied by QCT.

We have determined the fluorescence decay profile of QCT in buffer and in the presence of POPC and POPC/cholesterol lipid bilayers. The fluorescence lifetime of QCT under these conditions is short, and in all three situations we have obtained a similar fluorescence lifetime for QCT, around 1 ns, with sub-nanosecond components (Table S2). This is in agreement with the visual inspection of the fluorescence decays, which are virtually indistinguishable, and with the similar fluorescence quantum yield of QCT in buffer and in the presence of the two lipid systems (Table S1). These results show that the changes in excited-state lifetime are not sufficient to justify the

differences obtained for the steady-state anisotropy of QCT. In fact, if we compare the anisotropy of QCT in buffer solution, ca. 0.08 with the values obtained for full incorporation in the membrane, it is clear that the measured values are reflecting the slower/more restricted rotation dynamics, as the anisotropy value is much higher in both lipid phases when compared to its value in buffer solution, despite the shorter fluorescence lifetime in the latter.

Table S2. Parameters describing quercetin fluorescence decays (8 µM) in HEPES buffer and LUV suspensions (1 mM total lipid) of POPC; POPC/Cholesterol 1:1. Values in the form mean ± standard deviation; p-value<0.05 *, versus quercetin in buffer.

System	α_1	τ_1 (ns)	α_2	τ_2 (ns)	α_3	τ_3 (ns)	$\bar{\tau}$ (ns)	$<\tau>$ (ns)
Buffer	1	0.86±0.06					0.86±0.06	0.86±0.06
POPC	0.70±0.16	0.70±0.22	0.30±0.16	1.47±0.21			0.93±0.09	1.07±0.04
POPC/Chol	0.49±0.05	0.50±0.04	0.50±0.05	1.16±0.04	0.012±0.005	5.02±0.67	0.88±0.01	1.23±0.03*

Note 3. Accessibility of quercetin to quenchers/oxidant agents

Quenching experiments were performed using lipid concentrations affording that, with both lipid systems, 83% of QCT is partitioned into the lipid (Figure S4).
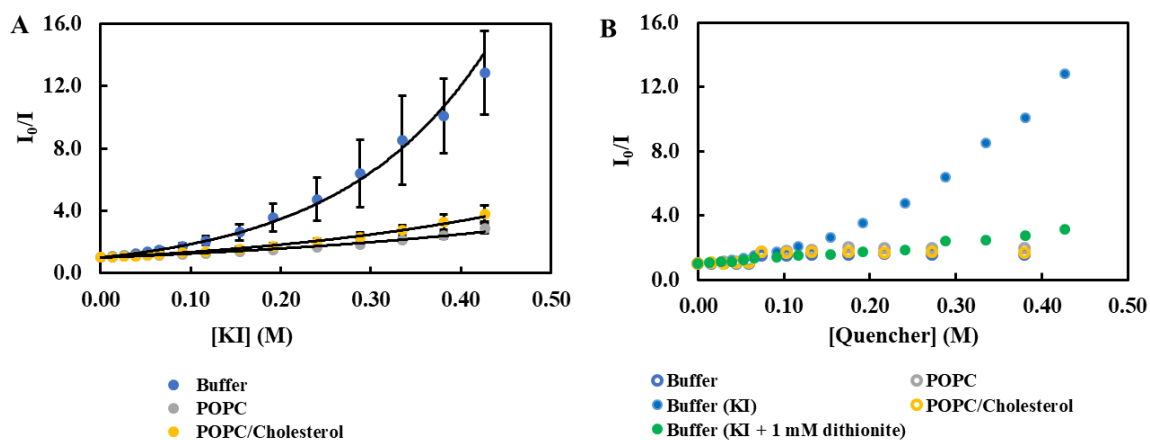
Figure S4. Stern-Volmer plot of quercetin steady-state fluorescence quenching. A. Quenching by [KI]. B. Quenching by acrylamide (empty circles) and KI in the absence and presence of the reducing agent sodium dithionite (full circles). Lipid concentrations were 0.4 mM (POPC) and 2.5 mM (POPC/Cholesterol 1:1). Quercetin concentration was 20 µM.

The formation of a ground state non-fluorescent complex between QCT and the quencher should give a linear Stern-Volmer plot. The exponential law should be valid for a static quenching based on the random chance of finding a quencher molecule in the molecular vicinity of a fluorophore when it undergoes a transition to the excited-state. However, this mechanism should be operative for acrylamide, and by itself does not justify the elimination of quenching by the reducing agent (dithionite). These quenching results can only be explained considering the involvement of a pseudo first-order redox process.

Note 4. Quercetin effect on membrane hydration and membrane surface dynamics

TMA-DPH fluorescence intensity decay is well described by the sum of 2 or 3 exponentials, in the absence or presence of QCT, respectively, in all systems (Table S3). A direct interaction between TMA-DPH and QCT has been ruled out in the work by Margina et al.[7] Furthermore, considering the hypothesis of a direct interaction between TMA-DPH and QCT being responsible for the decrease in the probe lifetime, this effect would be stronger in POPC, because QCT partition is more efficient to this lipid system than to the others; also, the short component lifetime that appears in the presence of QCT, is characteristic of water penetration, and is similar to the fluorescence lifetime of the probe in water. More interestingly, the longer component lifetime (Table S3) is not affected by QCT in POPC bilayers, but it is considerably shortened in the more ordered and less hydrated bilayers to the value determined in the control of POPC bilayers. This effect is analogous to the one in NBD-DOPE fluorescence anisotropy, and the lifetime of this probe was practically unaffected by QCT.

Table S3. Parameters describing TMA-DPH fluorescence decays in LUV (1 mM total lipid) of POPC; POPC/Chol (1:1) and POPC/PSM/Chol (1:1:1), in control and with 80 μM of quercetin. All points are the average of at least 3 independent measurements ± standard deviation of the mean.

System	α_1	τ_1 (ns)	α_2	τ_2 (ns)	α_3	τ_3 (ns)	$\bar{\tau}$ (ns)	$\langle\tau\rangle$ (ns)
POPC								
Control			0.27±0.06	1.77±0.35	0.73±0.06	4.81±0.06	4.00±0.04	4.45±0.06
Quercetin	0.70±0.06	0.74±0.22	0.27±0.03	1.79±0.48	0.04±0.02	4.44±0.55	1.14±0.43	1.58±0.60
POPC/Chol (1:1)								
Control			0.11±0.01	3.58±0.23	0.89±0.01	8.15±0.16	7.67±0.13	7.92±0.14
Quercetin	0.59±0.02	0.87±0.07	0.34±0.02	2.03±0.09	0.07±0.01	4.37±0.31	1.51±0.08	2.11±0.17
POPC/PSM/Chol (1:1:1)								
Control			0.11±0.01	2.71±0.90	0.89±0.01	8.07±0.11	7.49±0.09	7.87±0.12
Quercetin	0.68±0.03	0.80±0.05	0.27±0.02	2.30±0.29	0.05±0.02	5.13±0.54	1.42±0.14	2.22±0.39

Changes in NBD-DOPE fluorescence decay parameters induced by QCT in the different lipid systems are shown in Figure S5 and Table S4.
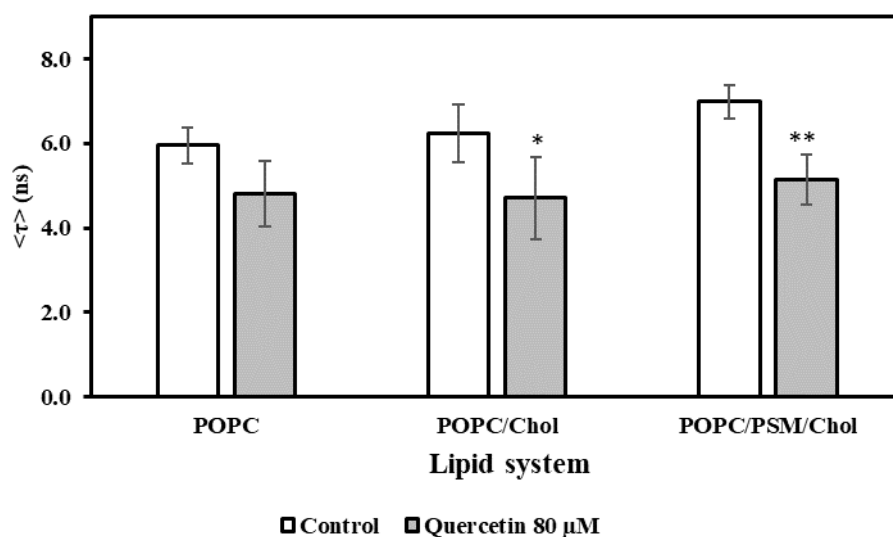
Figure S5. Intensity weighted mean fluorescence lifetime of NBD-DOPE in LUV (1 mM total lipid) of POPC; POPC/Chol and POPC/PSM/Chol) for 0 (white bars) and 80 μM (grey bars) of quercetin. All points are the average of at least 3 independent measurements ± standard deviation of the mean. *p*-value<0.05 *; *p*-value<0.01 **.

Table S4. Parameters describing NBD-DOPE fluorescence decays in LUV (1 mM total lipid) of POPC; POPC/Chol (1:1) and POPC/PSM/Chol (1:1:1), in control and in presence of 80 µM of quercetin. All values are the average of at least 3 independent measurements ± standard deviation of the mean. *p*-value<0.05 *; *p*-value<0.01 **

System	α_1	τ_1 (ns)	α_2	τ_2 (ns)	$\bar{\tau}$ (ns)	$<\tau>$ (ns)
POPC						
Control	0.78±0.02	1.18±0.08	0.22±0.02	8.37±0.45	2.74±0.25	5.96±0.43
Quercetin	0.85±0.03	1.21±0.07	0.15±0.03	7.85±0.57	2.25±0.35	4.81±0.77
POPC/Chol (1:1)						
Control	0.83±0.04	1.18±0.05	0.17±0.04	9.48±0.23	2.56±0.41	6.23±0.68
Quercetin	0.89±0.04	1.15±0.08	0.11±0.04	8.53±0.46**	2.00±0.43	4.70±0.97*
POPC/PSM/Chol (1:1:1)						
Control	0.85±0.02	1.20±0.05	0.15±0.02	10.70±0.31	2.63±0.23	6.98±0.39
Quercetin	0.91±0.02	1.18±0.06	0.09±0.02	9.80±0.39*	1.99±0.22**	5.15±0.60**

Note 5. Properties of the lipid bilayers from MD simulations

The effects of QCT on membrane structure were evaluated by comparing the lipid order parameter (S_{CD}) of pure membranes with that of the lipid molecules in the vicinity of QCT, as shown in Figure S6. This local S_{CD} calculation was performed only for the POPC molecules whose centre of mass (COM) was at 0.6 nm from the COM of QCT molecules, at any time during the simulation time. In POPC membranes QCT reduces the order of the *sn-1* chain, with higher effect at the mid chain carbons. For the *sn-2* chain QCT shows a different effect. It orders the first chain carbons while disordering those closer to the bilayer centre. In POPC/Cholesterol membranes a disordering effect of QCT was obtained for both lipid chains, more noticeable until the seventh carbon region. The decrease of the order parameter for the phospholipids neighbouring the QCT molecules indicates its effect in perturbing the structure of the lipid membrane, namely for membranes in the ordered state.

The MD simulations were also analysed in order to assess the water penetration in the lipid bilayer. However, we were not able to find evidence for deeper water penetration in the presence of QCT. This result is probably consequence of the small number of QCT molecules used, which is not enough to generate large deformations in the membrane in order to increase significantly water penetration, being able, however, to locally change the order parameter profile of the lipids.
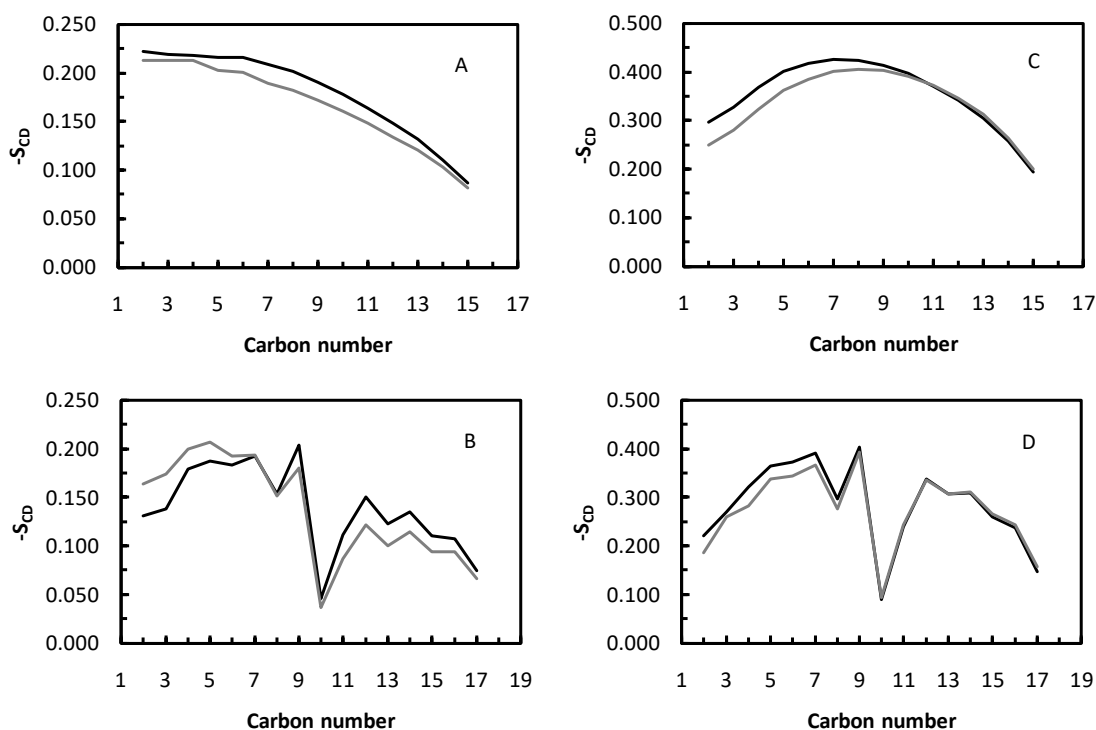
Figure S6. Influence of quercetin in order parameter (S_{CD}) for the carbons of each POPC chain, *sn*-1 (A, C) and *sn*-2 (B, D) in POPC (A, B) and POPC/Cholesterol (C, D) membranes. The S_{CD} profiles for the pure membrane systems (black lines) are compared to the S_{CD} profiles for the phospholipids in the vicinity of quercetin during the simulations (grey lines).

Another property that sheds light on the interaction of QCT with the lipid membranes is the possibility to establish hydrogen bonds. As shown in Figure S7, QCT is able to H-bond with all other constituents of the membrane systems, namely POPC, cholesterol and water. In the POPC/Cholesterol membranes a large number of hydrogen bonds with cholesterol was indeed identified. This indicates a possibility to disturb the POPC/Cholesterol H-bonding network contributing to disorder the membrane structure. The presence of QCT resulted in the reduction of H-bonding between POPC and cholesterol (Fig. S8).

POPC, Chol and water acceptors
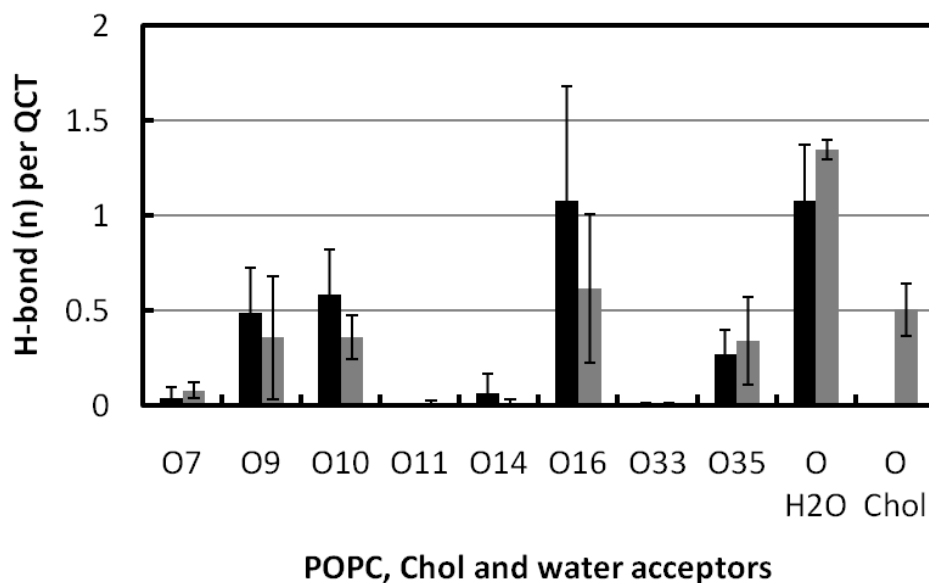
Figure S7. Average number of instant H-bonds per quercetin molecule between quercetin (donor) and POPC, water and Chol (acceptors). Black bars refer to POPC while grey bars refer to POPC/Cholesterol (1:1) membranes. The first eight set of columns refer to each individual O atom of POPC (see Fig. S1 for atom numbering). Data represents the average of all molecules and replicates for each simulated membrane system.
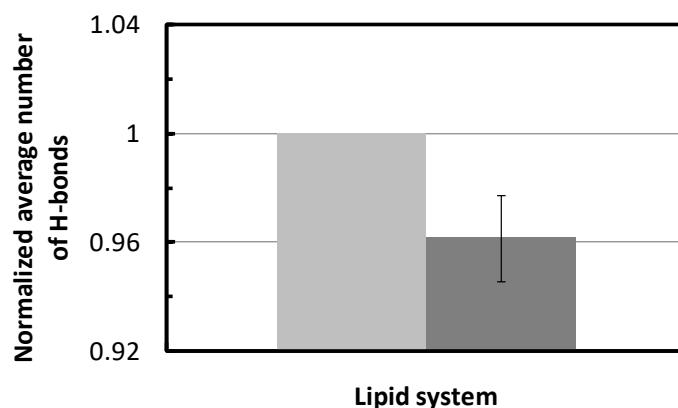
Figure S8. Normalized average number of instant H-bonds between Cholesterol (donor) and POPC (acceptor) for the POPC/Cholesterol bilayer without (light grey) and in presence of quercetin (grey). Regarding the presence of quercetin, the data represents the average of all molecules and replicates for the system, while for the pure bilayer it refers to a single control simulation at equilibrium.

The simulations above were all performed with the neutral form of QCT, although, as described under ESI Note 1, the predominant form may be the ionized one. This choice was made by three main reasons: i) in general, uncharged molecules tend to locate more deeply in the lipid membranes than charged ones. Therefore, it is more probable to reach the equilibrium configuration within a reasonable simulation time with neutral QCT; ii) as described above and in the main text, the molecular details of the interaction of QCT with the lipid membranes, including those behind membrane perturbation, and the relative location in POPC versus POPC/Chol bilayers, could be obtained simulating the neutral molecule; iii) on another hand, as stated under ESI Note 1, the extensive delocalization of the negative charge of the unprotonated QCT throughout the molecule renders the effect of total charge much milder than if the charge were mostly localized.

We cannot completely rule out that some differences could be obtained if the ionized QCT had been simulated, namely regarding the H-bonding patterns, and water penetration, since one of the five hydroxyl groups loses its H-bond donor ability. Nevertheless, even in this situation, QCT molecules maintain a large number of protonated OH groups.

Note 6. Topology file for QUERCETIN (QCT) (Gromos 54a7 force field)

[moleculetype]
; Name   nrexcl
QCT   3
[atoms]
; nr type resnr resid atom cgnr charge   mass
  1 HS14 1   QCT   H1   1 0.431 1.0080
  2 OA   1   QCT   O2   1 -0.569 15.9994
  3 C   1   QCT   C3   1 0.548 12.0110
  4 C   1   QCT   C4   1 -0.530 12.0110
  5 HC   1   QCT   H5   1 0.236 1.0080
  6 C   1   QCT   C6   2 -0.630 12.0110
  7 HC   1   QCT   H7   2 0.195 1.0080
  8 C   1   QCT   C8   2 0.522 12.0110
  9 OE   1   QCT   O9   2 -0.228 15.9994
 10 C   1   QCT   C10 3 0.089 12.0110
 11 C   1   QCT   C11 3 0.132 12.0110
 12 C   1   QCT   C12 3 -0.247 12.0110
 13 HC   1   QCT   H13 3 0.169 1.0080
 14 C   1   QCT   C14 3 -0.029 12.0110
 15 OA   1   QCT   O15 3 -0.468 15.9994
 16 H   1   QCT   H16 3 0.384 1.0080
 17 C   1   QCT   C17 4 -0.380 12.0110
 18 HC   1   QCT   H18 4 0.167 1.0080
 19 C   1   QCT   C19 4 0.263 12.0110
 20 OA   1   QCT   O20 4 -0.606 15.9994
 21 HS14 1   QCT   H21 4 0.461 1.0080
 22 C   1   QCT   C22 5 0.283 12.0110
 23 OA   1   QCT   O23 5 -0.530 15.9994
 24 HS14 1   QCT   H24 5 0.440 1.0080
 25 C   1   QCT   C25 5 -0.242 12.0110
 26 HC   1   QCT   H26 5 0.190 1.0080
 27 C   1   QCT   C27 6 0.577 12.0110
 28 OA   1   QCT   O28 6 -0.571 15.9994
 29 HS14 1   QCT   H29 6 0.434 1.0080
 30 C   1   QCT   C30 6 -0.625 12.0110
 31 C   1   QCT   C31 6 0.662 12.0110
 32 O   1   QCT   O32 6 -0.528 15.9994
; total charge of the molecule: 0.000
[bonds]
; ai aj funct c0   c1
  1   2   2 0.0972 1.9581e+07
  2   3   2 0.1360 1.0200e+07
  3   4   2 0.1400 8.5400e+06
  3   6   2 0.1390 8.6600e+06
  4   5   2 0.1090 1.2300e+07
  4 27   2 0.1390 8.6600e+06
  6   7   2 0.1090 1.2300e+07
  6   8   2 0.1390 8.6600e+06
  8   9   2 0.1360 1.0200e+07
  8 30   2 0.1400 8.5400e+06
  9 10   2 0.1380 1.1000e+07
 10 11   2 0.1470 8.7100e+06
 10 14   2 0.1360 1.0200e+07
 11 12   2 0.1400 8.5400e+06
 11 17   2 0.1410 6.5389e+06
 12 13   2 0.1090 1.2300e+07
 12 25   2 0.1390 8.6600e+06
 14 15   2 0.1360 1.0200e+07
 14 31   2 0.1460 4.6913e+06
 15 16   2 0.0972 1.9581e+07
 17 18   2 0.1090 1.2300e+07
 17 19   2 0.1390 8.6600e+06

```
 19  20   2  0.1360  1.0200e+07
 19  22   2  0.1410  6.5389e+06
 20  21   2  0.0972  1.9581e+07
 22  23   2  0.1360  1.0200e+07
 22  25   2  0.1390  8.6600e+06
 23  24   2  0.0972  1.9581e+07
 25  26   2  0.1090  1.2300e+07
 27  28   2  0.1350  1.0300e+07
 27  30   2  0.1430  8.1800e+06
 28  29   2  0.1000  1.5700e+07
 30  31   2  0.1450  5.2319e+06
 31  32   2  0.1250  1.3400e+07
[ pairs ]
; ai  aj  funct ; all 1-4 pairs but the ones excluded in GROMOS itp
  9  15   1
 15  30   1
 15  32   1
 28  31   1
  2   5   1
  2   7   1
  2   8   1
  2  27   1
 20  23   1
 20  25   1
 23  26   1
  8  28   1
  8  32   1
 10  13   1
 10  16   1
 10  18   1
 10  32   1
 11  15   1
 11  20   1
 11  26   1
 27  32   1
  3  28   1
 17  21   1
 17  23   1
  4   7   1
  4  29   1
 12  18   1
 12  23   1
 19  24   1
 19  26   1
  7   9   1
  7  30   1
 18  20   1
 18  22   1
  5   6   1
  5  28   1
  5  30   1
 13  17   1
 13  22   1
 13  26   1
 16  31   1
 29  30   1
  1   4   1
  1   6   1
 21  22   1
 24  25   1
[ angles ]
; ai  aj  ak funct  angle    fc
  1   2   3   2  109.50  450.00
```

```
 2   3   4   2   121.00   685.00
 2   3   6   2   117.00   635.00
 4   3   6   2   120.00   560.00
 3   4   5   2   120.00   505.00
 3   4   27  2   120.00   560.00
 5   4   27  2   120.00   505.00
 3   6   7   2   120.00   505.00
 3   6   8   2   120.00   560.00
 7   6   8   2   120.00   505.00
 6   8   9   2   117.00   635.00
 6   8   30  2   120.00   560.00
 9   8   30  2   121.00   685.00
 8   9   10  2   121.40   690.00
 9   10  11  2   111.00   530.00
 9   10  14  2   121.00   685.00
 11  10  14  2   126.00   640.00
 10  11  12  2   120.00   560.00
 10  11  17  2   120.00   560.00
 12  11  17  2   120.00   560.00
 11  12  13  2   120.00   505.00
 11  12  25  2   120.00   560.00
 13  12  25  2   120.00   505.00
 10  14  15  2   126.00   640.00
 10  14  31  2   120.00   560.00
 15  14  31  2   115.00   610.00
 14  15  16  2   109.50   450.00
 11  17  18  2   120.00   505.00
 11  17  19  2   120.00   560.00
 18  17  19  2   120.00   505.00
 17  19  20  2   126.00   640.00
 17  19  22  2   120.00   560.00
 20  19  22  2   115.00   610.00
 19  20  21  2   109.50   450.00
 19  22  23  2   121.00   685.00
 19  22  25  2   120.00   560.00
 23  22  25  2   120.00   560.00
 22  23  24  2   109.50   450.00
 12  25  22  2   120.00   560.00
 12  25  26  2   120.00   505.00
 22  25  26  2   120.00   505.00
 4   27  28  2   120.00   560.00
 4   27  30  2   120.00   560.00
 28  27  30  2   120.00   560.00
 27  28  29  2   109.50   450.00
 8   30  27  2   120.00   560.00
 8   30  31  2   120.00   560.00
 27  30  31  2   120.00   560.00
 14  31  30  2   111.00   530.00
 14  31  32  2   121.00   685.00
 30  31  32  2   121.00   685.00
[ dihedrals ]
; GROMOS improper dihedrals
; ai  aj  ak  al funct  angle    fc
 30   8  31  27  2    0.00  167.36
  8   9  30   6  2    0.00  167.36
 10   9  11  14  2    0.00  167.36
 11  10  17  12  2    0.00  167.36
 14  15  10  31  2    0.00  167.36
 31  32  30  14  2    0.00  167.36
 27  28  30   4  2    0.00  167.36
  6   8   3   7  2    0.00  167.36
  3   2   6   4  2    0.00  167.36
 17  11  19  18  2    0.00  167.36
```

```
  4  27   3   5   2    0.00  167.36
 12  11  25  13   2    0.00  167.36
 19  20  17  22   2    0.00  167.36
 25  12  22  26   2    0.00  167.36
 22  23  19  25   2    0.00  167.36
[ dihedrals ]
; ai  aj  ak  al funct  ph0    cp    mult
  1   2   3   6   1  180.00   16.70  2
  6   3   4  27   1  180.00   41.80  2
  4   3   6   8   1  180.00   41.80  2
  3   4  27  30   1  180.00   41.80  2
  3   6   8  30   1  180.00   41.80  2
 30   8   9  10   1  180.00   41.80  2
  6   8  30  27   1  180.00   41.80  2
  8   9  10  14   1  180.00   41.80  2
  9  10  11  17   1  180.00    5.86  2
  9  10  14  31   1  180.00   41.80  2
 17  11  12  25   1  180.00   41.80  2
 12  11  17  19   1  180.00   41.80  2
 11  12  25  22   1  180.00   41.80  2
 10  14  15  16   1  180.00   16.70  2
 10  14  31  30   1  180.00   41.80  2
 11  17  19  22   1  180.00   41.80  2
 17  19  20  21   1  180.00   16.70  2
 17  19  22  25   1  180.00   41.80  2
 19  22  23  24   1  180.00   16.70  2
 19  22  25  12   1  180.00   41.80  2
 30  27  28  29   1  180.00   16.70  2
  4  27  30   8   1  180.00   41.80  2
  8  30  31  14   1  180.00   41.80  2
[ exclusions ]
; ai  aj funct ; GROMOS 1-4 exclusions
  9  12
  9  17
  9  27
  9  31
  8  11
  8  14
 10  19
 10  25
 10  30
 11  22
 11  31
 14  17
 14  27
  6  10
  6  27
  6  31
  3   9
  3  30
 17  25
  4   8
  4  31
 12  14
 12  19
```

References

1. H. A. L. Filipe, C. Sousa, J. T. Marquês, D. Vila-Viçosa, A. de Granada-Flor, A. S. Viana, M. S. C. S. Santos, M. Machuqueiro and R. F. M. de Almeida, *Free Rad. Biol. Med.*, 2018, **115**, 232-245.
2. R. F. M. de Almeida, A. Fedorov and M. Prieto, *Biophys. J.*, 2003, **85**, 2406-2416.
3. J. R. Lakowicz, *Principles of fluorescence spectroscopy*, Springer, NY USA, 3rd edn., 2006.
4. C. R. Mateo, R. F. M. de Almeida, L. M. S. Loura and M. Prieto, in *Protein-Lipid Interactions: New Approaches and Emerging Concepts*, eds. C. R. Mateo, J. Gómez, J. Villalaín and J. M. González-Ros, Springer Berlin Heidelberg, 2006, pp. 1-33.
5. L. Grönberg, J. P. Slotte, Z. S. Ruan and R. Bittman, *Biochemistry*, 1991, **30**, 10746-10754.
6. D. Marsh, *Handbook of Lipid Bilayers*, CRC Press, 2nd edn., 2013.
7. D. Margina, M. Ilie and D. Gradinaru, *Int. J. Mol. Sci.*, 2012, **13**, 4839-4859.
8. S. Pronk, S. Páll, R. Schulz, P. Larsson, P. Bjelkmar, R. Apostolov, M. R. Shirts, J. C. Smith, P. M. Kasson, D. van der Spoel, B. Hess and E. Lindahl, *Bioinformatics*, 2013, **29**, 845-854.
9. N. Schmid, A. P. Eichenberger, A. Choutko, S. Riniker, M. Winger, A. E. Mark and W. F. van Gunsteren, *Eur. Biophys. J.*, 2011, **40**, 843-856.
10. W. R. P. Scott, P. H. Hünenberger, I. G. Tironi, A. E. Mark, S. R. Billeter, J. Fennen, A. E. Torda, T. Huber, P. Krüger and W. F. van Gunsteren, *J. Phys. Chem. A*, 1999, **103**, 3596-3607.
11. W. F. v. Gunsteren, X. Daura and A. E. Mark, *Encyclopedia of Computational Chemistry*, John Wiley & Sons, Ltd, 2002.
12. J. Hermans, H. J. C. Berendsen, W. F. Van Gunsteren and J. P. M. Postma, *Biopolymers*, 1984, **23**, 1513-1518.
13. K. B. Koziara, M. Stroet, A. K. Malde and A. E. Mark, *J. Comput. Aided Mol. Des.*, 2014, **28**, 221-233.
14. A. K. Malde, L. Zuo, M. Breeze, M. Stroet, D. Poger, P. C. Nair, C. Oostenbrink and A. E. Mark, *J. Chem. Theory Comput.*, 2011, **7**, 4026-4037.
15. B. H. Besler, K. M. Merz and P. A. Kollman, *J. Comput. Chem.*, 1990, **11**, 431-439.
16. M. S. Gordon and M. W. Schmidt, in *Theory and Applications of Computational Chemistry: the first forty years*, 2005, pp. 1167-1189.
17. M. W. Schmidt, K. K. Baldridge, J. A. Boatz, S. T. Elbert, M. S. Gordon, J. H. Jensen, S. Koseki, N. Matsunaga, K. A. Nguyen, S. Su, T. L. Windus, M. Dupuis and J. A. Montgomery, *J. Comput. Chem.*, 1993, **14**, 1347-1363.
18. A. D. Becke, *J. Chem. Phys.*, 1993, **98**, 5648-5652.
19. C. Lee, W. Yang and R. G. Parr, *Phys. Rev. B*, 1988, **37**, 785-789.
20. S. H. Vosko, L. Wilk and M. Nusair, *Can. J. Phys.*, 1980, **58**, 1200-1211.
21. P. C. Hariharan and J. A. Pople, *Theor. Chim. Acta*, 1973, **28**, 213-222.
22. H. A. L. Filipe, D. Bowman, T. Palmeira, R. M. S. Cardoso, L. M. S. Loura and M. J. Moreno, *Phys. Chem. Chem. Phys.*, 2015, **17**, 27534-27547.
23. S. Miyamoto and P. A. Kollman, *J. Comput. Chem.*, 1992, **13**, 952-962.
24. B. Hess, H. Bekker, H. J. C. Berendsen and J. G. E. M. Fraaije, *J. Comput. Chem.*, 1997, **18**, 1463-1472.
25. H. J. C. Berendsen, J. P. M. Postma, W. F. v. Gunsteren, A. DiNola and J. R. Haak, *J. Chem. Phys.*, 1984, **81**, 3684-3690.
26. G. Bussi, D. Donadio and M. Parrinello, *J. Chem. Phys.*, 2007, **126**, 014101.
27. U. Essmann, L. Perera, M. L. Berkowitz, T. Darden, H. Lee and L. G. Pedersen, *J. Chem. Phys.*, 1995, **103**, 8577-8593.
28. W. Humphrey, A. Dalke and K. Schulten, *J. Mol. Graph.*, 1996, **14**, 33-38.
29. C. W. McClare, *Anal. Biochem.*, 1971, **39**, 527-530.

30. L. C. Silva, R. F. M. de Almeida, B. M. Castro, A. Fedorov and M. Prieto, *Biophys. J.*, 2007, **92**, 502-516.
31. S. N. Pinto, L. C. Silva, R. F. M. De Almeida and M. Prieto, *Biophys. J.*, 2008, **95**, 2867-2879.
32. G. M. Escandar and L. F. Sala, *Can. J. Chem.*, 1991, **69**, 1994-2001.
33. J. M. Herrero-Martínez, M. Sanmartin, M. Rosés, E. Bosch and C. Ràfols, *Electrophoresis*, 2005, **26**, 1886-1895.
34. M. Musialik, R. Kuzmicz, T. S. Pawlowski and G. Litwinienko, *J. Org. Chem.*, 2009, **74**, 2699-2709.
35. A. Mezzetti, S. Protti, C. Lapouge and J. P. Cornard, *Phys. Chem. Chem. Phys.*, 2011, **13**, 6858-6864.
36. V. H. Teixeira, D. Vila-Vicosa, P. B. Reis and M. Machuqueiro, *J. Chem. Theory Comput.*, 2016, **12**, 930-934.
37. A. E. P. Bastos, H. S. Marinho, A. M. Cordeiro, A. M. de Soure and R. F. M. de Almeida, *Chem. Phys. Lipids*, 2012, **165**, 577-588.
38. R. M. Cardoso, H. A. Filipe, F. Gomes, N. D. Moreira, W. L. Vaz and M. J. Moreno, *J. Phys. Chem. B*, 2010, **114**, 16337-16346.